Mutation of *Arabidopsis SMC4* identifies condensin as a corepressor of pericentromeric transposons and conditionally expressed genes

Jing Wang,[1,2] Todd Blevins,[1,2,3,6] Ram Podicheti,[4,5] Jeremy R. Haag,[7] Ek Han Tan,[8] Feng Wang,[1,2] and Craig S. Pikaard[1,2,3]

[1]Department of Biology, Indiana University, Bloomington, Indiana, 47405, USA; [2]Department of Molecular and Cellular Biochemistry, Indiana University, Bloomington, Indiana, 47405, USA; [3]Howard Hughes Medical Institute, Indiana University, Bloomington, Indiana, 47405, USA; [4]Center for Genomics and Bioinformatics, Indiana University, Bloomington, Indiana, 47405, USA; [5]School of Informatics and Computing, Indiana University, Bloomington, Indiana, 47405, USA

In eukaryotes, transcriptionally inactive loci are enriched within highly condensed heterochromatin. In plants, as in mammals, the DNA of heterochromatin is densely methylated and wrapped by histones displaying a characteristic subset of post-translational modifications. Growing evidence indicates that these chromatin modifications are not sufficient for silencing. Instead, they are prerequisites for further assembly of higher-order chromatin structures that are refractory to transcription but not fully understood. We show that silencing of transposons in the pericentromeric heterochromatin of *Arabidopsis thaliana* requires SMC4, a core subunit of condensins I and II, acting in conjunction with CG methylation by MET1 (DNA METHYLTRANSFERASE 1), CHG methylation by CMT3 (CHROMOMETHYLASE 3), the chromatin remodeler DDM1 (DECREASE IN DNA METHYLATION 1), and histone modifications, including histone H3 Lys 27 monomethylation (H3K27me1), imparted by ATXR5 and ATXR6. SMC4/condensin also acts within the mostly euchromatic chromosome arms to suppress conditionally expressed genes involved in flowering or DNA repair, including the DNA glycosylase ROS1, which facilitates DNA demethylation. Collectively, our genome-wide analyses implicate condensin in the suppression of hundreds of loci, acting in both DNA methylation-dependent and methylation-independent pathways.

[*Keywords*: DNA methylation; SMC proteins; chromosome condensation; epigenetic regulation; gene silencing; heterochromatin formation]

Supplemental material is available for this article.

Received May 5, 2017; revised version accepted August 7, 2017.

Condensins are multisubunit protein complexes named for their ability to catalyze ATP-dependent condensation of newly replicated chromosomes (Wood et al. 2010; Hirano 2016; Uhlmann 2016). Two condensin subtypes (I and II) have at their core a heterodimer of the STRUCTURAL MAINTENANCE OF CHROMOSOMES (SMC) ATPases SMC2 and SMC4, which are highly conserved and essential for viability. Three additional subunits, each having paralogs that differ in condensins I and II, interact with the SMC2–SMC4 heterodimers, forming pentameric complexes that can topologically entrap DNA sequences brought together by looping, loop stacking, or other long-range interactions, thereby compacting the DNA. In addition to roles in mitosis, condensins affect genome organization and recombination and DNA repair, with a number of studies also implicating condensin in the repression of specific genes (Lupo et al. 2001; Bhalla et al. 2002; Dej et al. 2004; Machin et al. 2004; Meyer 2010; Wood et al. 2010; Rawlings et al. 2011; Jeppsson et al. 2014; He et al. 2016).

Much of what is known about condensin's effects on gene regulation stems from studies conducted using yeast,

Present addresses: [6]UPR 2357, Institut de Biologie Moléculaire des Plantes, Centre National de la Recherche Scientifique, Université de Strasbourg, F-67000 Strasbourg, France; [7]Monsanto Company, Chesterfield, MO 63017, USA; [8]School of Biology and Ecology, University of Maine, Orono, ME 04469, USA.
Corresponding author: cpikaard@indiana.edu
Article published online ahead of print. Article and publication date are online at http://www.genesdev.org/cgi/doi/10.1101/gad.301499.117.

Drosophila, or *Caenorhabditis elegans,* whose genomes lack appreciable DNA methylation. However, genomic cytosine methylation is common in eukaryotes, including plants and mammals (Law and Jacobsen 2010). The majority of cytosine methylation occurs at CG motifs and is accomplished by orthologous enzymes in mammals and plants; namely, the cytosine methyltransferases DNMT1 (DNA METHYLTRANSFERASE 1; mammals) or MET1 (plants). CG motifs are symmetrical in duplex DNA, and hemimethylated pairs of CG motifs are recognized by UHRF (mammals) or VIM (plants) proteins to facilitate DNMT1 or MET1 recruitment, thereby maintaining methylation on both strands (Bostick et al. 2007; Woo et al. 2007; Hashimoto et al. 2008). CHG methylation (where H is A, C, or T) is also symmetric and can be maintained in *Arabidopsis* by CMT3 (CHROMOMETHYLASE 3). CMT3 has a chromodomain that binds histone H3 Lys9 (H3K9) dimethylated by SUVH4 (or related paralogs), and SUVH4 in turn binds methylated CHG, allowing CHG methylation and H3K9 methylation (H3K9me) to specify and maintain one another (Law and Jacobsen 2010).

Pericentromeric regions account for most of the constitutive heterochromatin in *Arabidopsis* (Fransz et al. 2002; Zhang et al. 2006). These regions are transposon-rich and gene-poor, with dense CG maintenance methylation required to keep the transposons inactive (Soppe et al. 2002; Lippman et al. 2004; Simon et al. 2015). However, transposons located elsewhere, particularly in the mostly euchromatic chromosome arms, require additional methylation by DRM2, the ortholog of mammalian DNMT3 enzymes. DRM2 methylates cytosines in CG, CHG, or CHH motifs in an RNA-directed manner (Cao and Jacobsen 2002; Cao et al. 2003; Zemach et al. 2013; Matzke and Mosher 2014; Wendte and Pikaard 2017). In some contexts, primarily pericentromeric heterochromatin, CHH methylation can be maintained by the DNA methyltransferase CMT2 (Zemach et al. 2013; Stroud et al. 2014). CG, CHG, and CHH maintenance methylation has at least one thing in common; namely, the need for the chromatin remodeling ATPase DDM1 (DECREASE IN DNA METHYLATION 1) (Jeddeloh et al. 1999; Brzeski and Jerzmanowski 2003), which enables maintenance methylation within regions of dense heterochromatin enriched for linker histone H1 (Zemach et al. 2013).

Here, we report a hitherto unrecognized role for condensins I and II in methylation-dependent repression of pericentromeric transposons whose silencing depends on MET1, CMT3, DDM1, and the H3K27 monomethylases ATXR5 and ATXR6 (Jacob et al. 2009, 2010). Cytosine methylation is not appreciably altered in *smc4* mutants, suggesting that condensin is not required for DNA methylation but acts in conjunction with DNA methylation to assemble higher-order repressive chromatin complexes. We also show that SMC4/condensin does not act solely at heavily methylated loci of pericentromeric regions but also represses sparsely methylated, conditionally expressed genes throughout the chromosome arms, suggesting a broad role in shaping the *Arabidopsis* epigenome.

Results

Overexpression of the NRPE1 C-terminal domain (CTD) results in defective RNA-directed DNA methylation (RdDM)

Our finding that SMC4/condensin regulates gene silencing came about unexpectedly through studies of RdDM, which involves two specialized multisubunit RNA polymerases: polymerase IV (Pol IV) and Pol V (Haag and Pikaard 2011; Matzke and Mosher 2014; Zhou and Law 2015; Wendte and Pikaard 2017). We found that overexpressing the CTD of the Pol V largest subunit, NRPE1, causes a dominant-negative phenotype resembling *nrpe1* loss-of-function mutants (Fig. 1). For instance, at 45S and 5S rRNA gene loci, Pol IV-dependent 24-nucleotide (nt) siRNAs that are diminished in a *nrpe1* mutant are similarly reduced in the *NRPE1 CTD* overexpression line *CTD-OX* (Fig. 1A). Likewise, RdDM at *AtSN1* and *SoloLTR* retrotransposons is lost in the *nrpe1-11* mutant and greatly reduced in *CTD-OX* plants, making the DNA of these elements susceptible to HaeIII or AluI digestion such that PCR amplification fails (Fig. 1B).

Knocking out both DRM2-mediated RdDM and CHG methylation by CMT3 causes overexpression of the F-box gene *SDC*, resulting in plants with elongated twisted leaves (Henderson and Jacobsen 2008). We found that *cmt3 CTD-OX* double mutants, like *drm1 drm2 cmt3* mutants, display strong *SDC* expression (Fig. 1C) and the characteristic twisted leaf phenotype (Fig. 1D). *AtSN1* and *soloLTR* retrotransposons are also highly expressed in *CTD-OX* plants, as in *nrpe1* mutants (Fig. 1C). We assayed endogenous *NRPE1* mRNA expression levels using both RT–PCR and quantitative RT–PCR (qRT–PCR) assays, detecting an increase in the *nrpd1-3* (pol IV) mutant but no change in *NRPE1* mRNA levels in *CTD-OX* plants (Fig. 1E; Supplemental Fig. S1A), suggesting CTD-OX interference with RdDM at a step downstream from *NRPE1* transcription.

Evidence that the CTD-OX *transgene induces RNAi*

Using a homozygous *cmt3 CTD-OX* line in which all progeny displayed the SDC phenotype, we conducted a suppressor screen. Seeds were subjected to EMS mutagenesis, and rare plants with a wild-type phenotype were identified in the next generation (M2). These plants no longer expressed *SDC*, as illustrated in Figure 1F for four such mutants (m17, m65, m71, and m73). In the mutants, *AtSN1* and *soloLTR* elements that had been derepressed in the *cmt3 CTD-OX* parental line (a *pol V* or RdDM mutant phenotype), were resilenced (Fig. 1F) and remethylated (Fig. 1G), and the CTD transgene remained expressed (Fig. 1F; Supplemental Fig. S1B), ruling out its silencing as the basis for the suppressor phenotype.

Evidence that recovered mutants were affecting more than one activity came from analyses of small RNAs. These included 24-nt siRNAs matching *5S* rRNA genes or *AtSN1* elements; 21-nt secondary siRNAs generated from *TAS1, TAS2*, or *TAS3* noncoding RNAs (Allen et al. 2005); or a 21-nt microRNA (*miR160*) (Fig. 2A). In

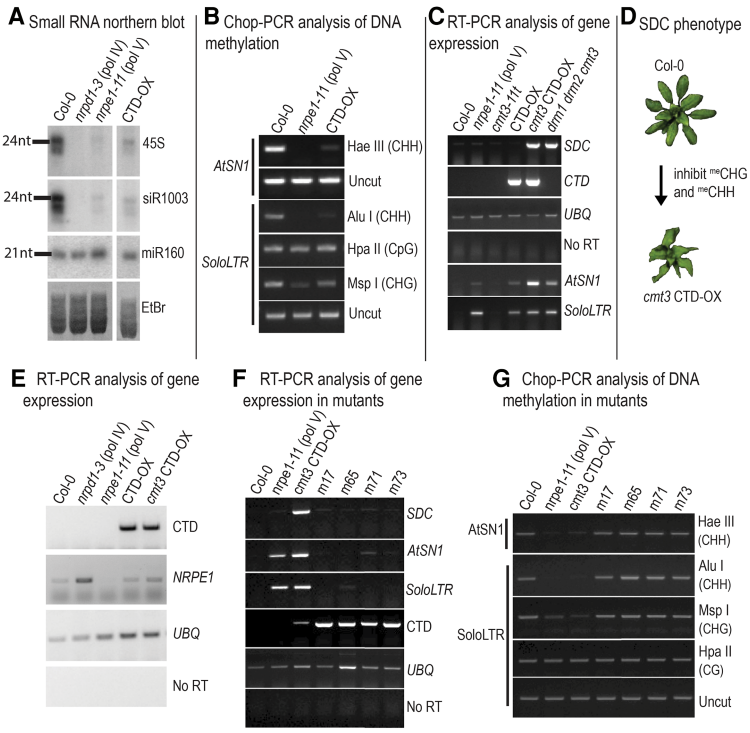

Figure 1. Overexpression of the Pol V largest subunit CTD induces a dominant-negative RdDM phenotype suppressed in EMS-induced mutants. (*A*) RNA blot analysis of small RNA of wild-type (Col-0), *pol IV* mutant (*nrpd1*), *pol V* mutant (*nrpe1-11*), or CTD-OX plants. The blot was sequentially probed for small RNAs matching the *45S* rRNA gene promoter, *5S* rRNA gene intergenic spacer (*siR1003*), or microRNA *miR160*. An image of the ethidium bromide (EtBr)-stained gel is shown at the *bottom*. (*B*) Analysis of *AtSN1* and *SoloLTR* transposon DNA methylation levels using Chop-PCR. Genomic DNA of wild-type Col-0, *Pol V* mutant (*nrpe1-11*), or CTD-OX plants was digested (chopped) with the indicated methylation-sensitive endonucleases (the sequence context of queried cytosines are shown in parentheses) or left uncut as a control and then amplified using PCR primers specific for *AtSN1* or *soloLTR* retrotransposons. PCR products were resolved by agarose gel electrophoresis and visualized with EtBr staining. (*C*) RT–PCR analyses of *SDC*, *CTD*, *AtSN1*, and *soloLTR* expression levels relative to a ubiquitin (*UBQ*) control. The genotypes of plants tested are indicated at the *top* of each lane. Reactions in which reverse transcriptase was omitted (no RT) control for DNA contamination. The *drm1 drm2 cmt3* genotype is known to induce *SDC* overexpression, serving as a positive control for the *cmt3 CTD-OX* genotype. The *CTD* reactions control for transgene expression. (*D*) CHG and CHH methylation-deficient *cmt3 CTD-OX* plants display the *SDC* overexpression phenotype. (*E*) RT–PCR analysis of *CTD* and native *NRPE1* expression. The genotypes of plants tested are indicated at the *top* of each lane. Reactions lacking reverse transcriptase (no RT) control for DNA contamination. *UBQ* reactions control for the amount of RNA tested. (*F*) RT–PCR analysis of *SDC*, *AtSN1*, *soloLTR*, and *CTD* expression in the *cmt3 CTD-OX* parental line and in the suppressor mutants m17, m65, m71, and m73. The *nrpe1-11* (*pol V*) mutant served as control for derepression of *AtSN1* and *SoloLTR* elements silenced by RdDM in wild type (Col-0). *UBQ* served as a loading control. Reactions without reverse transcriptase (no RT) served as controls for DNA contamination. (*G*) Analysis of *AtSN1* and *SoloLTR* DNA methylation levels using Chop-PCR. Assays were conducted as in *B*, comparing wild-type Col-0 with the indicated mutants.

all four mutants, 24-nt siRNAs increased from *pol V* (*nrpe1*) mutant levels to wild-type levels, but, in m17, *TAS* locus siRNAs (tasiRNAs) were absent. Production of tasiRNAs requires RNA-DEPENDENT RNA POLYMERASE 6 (RDR6) to generate the double-stranded precursors that are then diced into 21-nt RNAs (Peragine et al. 2004; Vazquez et al. 2004; Allen et al. 2005). This prompted genetic tests that revealed that mutant m17 is not complemented upon crossing to an *rdr6* mutant (see Supplemental Fig. S2A,B). Subsequent sequencing of the *RDR6* gene in m17 revealed a G-to-A transition, changing Gly866 to a glutamate at the enzyme's active site (Fig. 2B), the same mutation as in previously identified *rdr6-13* and *sgs2-6* alleles (Mourrain et al. 2000; Peragine et al. 2004). Additional genetic tests revealed that mutation of *SGS3*, which enables RDR6 function (Peragine et al. 2004; Vazquez et al. 2004), also suppresses *SDC, AtSN1*, and *soloLTR* expression in *cmt3 CTD-OX* plants (Supplemental Fig. S2C), as does mutation of *ARGONAUTE 1* (*AGO1*) (Supplemental Fig. S2D), which binds 21-nt siRNAs (Mallory and Vaucheret 2010).

Although *NRPE1* expression levels are not appreciably affected by the *CTD-OX* transgene (see Fig. 1E; Supplemental Fig. S1), the fact that *rdr6, sgs3,* and *ago1* mutations prevent *SDC, AtSN1*, and *soloLTR* overexpression in *cmt3 CTD-OX* plants strongly implicated 21-nt siRNA-mediated RNAi as the basis for *CTD-OX* action. This led us to examine whether 21-nt siRNAs matching the *NRPE1* CTD are produced in *cmt3 CTD-OX* plants but lost in the mutants. Indeed, this is the case, as shown in Figure 2C.

A missense allele of the condensin subunit gene SMC4 *suppresses the SDC phenotype*

Unlike the *rdr6* mutant (m17), mutant m73 showed no loss of 21-nt tasiRNAs (Fig. 2A) yet had lost 21-nt siRNAs matching the *NRPE1* CTD (Fig. 2C), suggesting a defect in transgene-induced RNAi but not tasiRNA biogenesis. The recessive nature of the m73 mutation and the dominant nature of the *CTD-OX* transgene for 21-nt siRNA production were evident upon crossing m73 with wild-type Col-0, yielding F1 progeny expressing high levels of 21-nt siRNAs matching the *NRPE1* CTD (Fig. 2C).

Using bulked-segregant analysis coupled with deep genome sequencing, the causative mutation in m73 was identified as a C-to-T transition in the *SMC4* gene (*AT5G48600*), defining the allele *smc4-1*. The missense mutation in *smc4-1* results in a proline-to-serine substitution at amino acid 22 (P22S) at the edge of the conserved

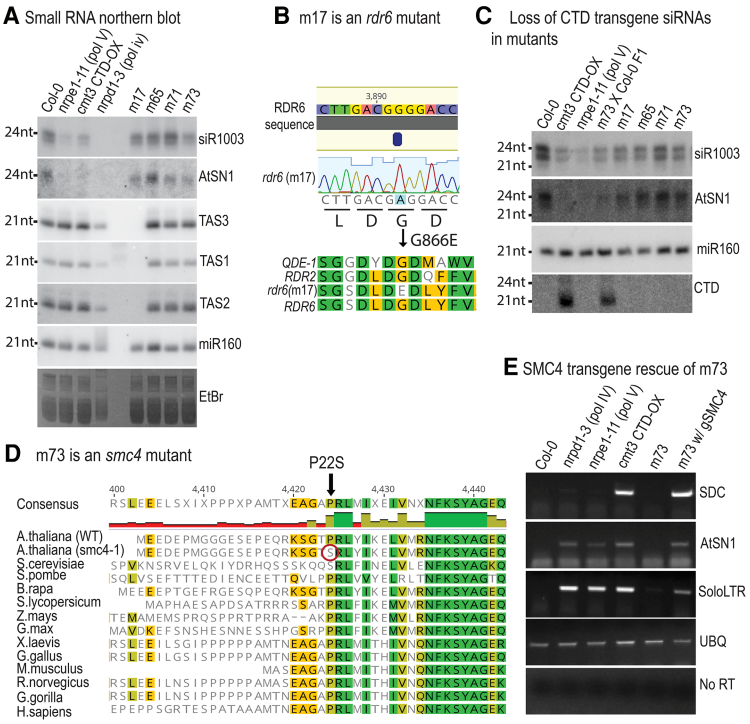

Figure 2. Suppressors of the SDC phenotype of *cmt3 CTD-OX* plants include mutant alleles for *RDR6* and the condensin core subunit *SMC4*. (*A*) Small RNA blot analyses. RNA isolated from the indicated genotypes was resolved by polyacrylamide gel electrophoresis and blotted to membranes that were then sequentially probed using body-labeled RNA oligonucleotides corresponding to the *5S* rRNA gene intergenic spacer (*siR1003*), *TAS3*, *TAS1*, *TAS2*, *miR160*, or *AtSN1*. The *nrpd1-3* (*pol IV*) and *nrpe1-11* (*pol V*) mutants were positive controls for loss or reduction, respectively, of 24-nt *siR1003* and *AtSN1* siRNAs. An image of the EtBr-stained gel is shown in the *bottom* panel. (*B*) Suppressor mutant m17 is an *rdr6* mutant. A guanosine-to-adenosine transition in the *RDR6* gene causes an amino acid change, G866E, in the enzyme active site. The multiple alignment compares active site regions of wild-type RDR6, m17 RDR6, *Neurospora* QDE-1, and *Arabidopsis* RDR2. (*C*) The *CTD-OX* transgene generates 21-nt CTD siRNAs that are lost in suppressor mutants. RNA blots for the indicated genotypes were sequentially probed for *siR1003* or *AtSN1* 24-nt siRNAs, *miR160*, or CTD small RNAs. (*D*) Mutant m73 harbors the mutant allele *smc4-1*. Multiple sequence alignment of the *SMC4* N-terminal region in diverse eukaryotes highlighting the P22S mutation present in suppressor mutant m73, defining the *smc4-1* allele. Identical amino acids are highlighted in green, and similar amino acids are highlighted in yellow. (*E*) *SMC4* transgene rescue of the *smc4-1* mutant. RT–PCR analyses of *SDC*, *AtSN1*, *SoloLTR*, and *UBQ* (control) expression in the indicated genotypes, including the *cmt3 CTD-OX* parental line used to conduct the suppressor screen, the m73 (*smc4-1*) mutant, and m73 transformed with an S*MC4* transgene (*gSMC4*) that reverts the expression pattern to that of the starting *cmt3 CTD-OX* line.

ATPase domain (Fig. 2D). Because a T-DNA insertion allele of *smc4* is embryonic-lethal when homozygous (Siddiqui et al. 2006; Smith et al. 2014), *smc4-1* is likely a hypomorphic allele.

To confirm that the *smc4-1* mutation is causative, we transformed the m73 mutant with a transgene expressing a full-length *SMC4* gene (*gSMC4*), which restored *SDC* expression (Fig. 2E). Likewise, *AtSN1* and *soloLTR* elements that had been silenced in the *smc4-1* (m73) mutant were again derepressed as in the starting *cmt3 CTD-OX* line (Fig. 2E) or in *nrpd1* (*pol IV*) or *nrpe1* (*pol V*) mutants.

Collectively, the results of the mutant screen are best explained by the interpretation that aberrant RNAs generated by the single-copy *CTD-OX* transgene give rise to RDR6- and SGS3-dependent 21-nt siRNAs that disrupt Pol V activity via RNAi. This impairs RdDM, resulting in *SDC*, *AtSN1*, and *soloLTR* expression. In the RNAi mutants, Pol V activity is no longer disrupted. We deduce that SMC4, as a key subunit of condensin, is somehow required for the *CTD-OX* transgene to produce aberrant RNAs.

To circumvent the uncertainties associated with the *cmt3 CTD-OX* genetic background, we outcrossed m73 to wild-type Col-0 and identified F2 progeny that were homozygous for *smc4-1*, homozygous wild-type for *CMT3*, and devoid of the *CTD-OX* transgene. These *smc4-1* homozygotes were further backcrossed twice to wild-type Col-0, yielding a homozygous line referred to here as *smc4-1* (Col-0) or simply *smc4-1*. This line was used for all subsequent assays.

SMC4 is required for pericentromeric transposon silencing and chromocenter condensation

Genome-wide effects of SMC4 on gene expression were investigated by conducting mRNA deep sequencing comparing *smc4-1* with wild-type plants. The most striking finding was that hundreds of transposable elements (TEs) are derepressed to high levels in *smc4-1* (Fig. 3A,B; Supplemental Table S1), most by a factor of ~16-fold to 100-fold compared with wild-type (Fig. 3B, note the $\log_2$ scale for the *Y*-axis). Nearly 80% are retrotransposons belonging to three superfamilies (LTR/gypsy, LTR/Copia, and Line/L1) (Fig. 3A), but En/Spm DNA transposons also represent a substantial subset. The derepressed TEs map primarily to the centromeric and pericentromeric regions of all five chromosomes (Fig. 3B) and tend to be long TEs, as categorized by Zemach et al. (2013) (Fig. 3C).

Using RT–PCR, we confirmed the derepression in *smc4-1* of several TEs identified by RNA sequencing (RNA-seq), comparing these with *soloLTR*, which is silenced by RdDM, while also testing a variety of mutants, including the RdDM mutants *nrpd1* (*pol IV*), *nrpe1* (*pol V*), and *drm1 drm2* or the maintenance methylation mutants *met1*, *cmt2*, and *cmt3* (Fig. 3D). Strikingly, TEs derepressed in *smc4-1* are also derepressed in *met1* or *cmt3* mutants but not in RdDM or *cmt2* mutants (Fig. 3D). Collectively, these results suggest that condensin is needed in addition to CG and CHG methylation for silencing of TEs located in pericentromeric heterochromatin. Consistent with this interpretation,

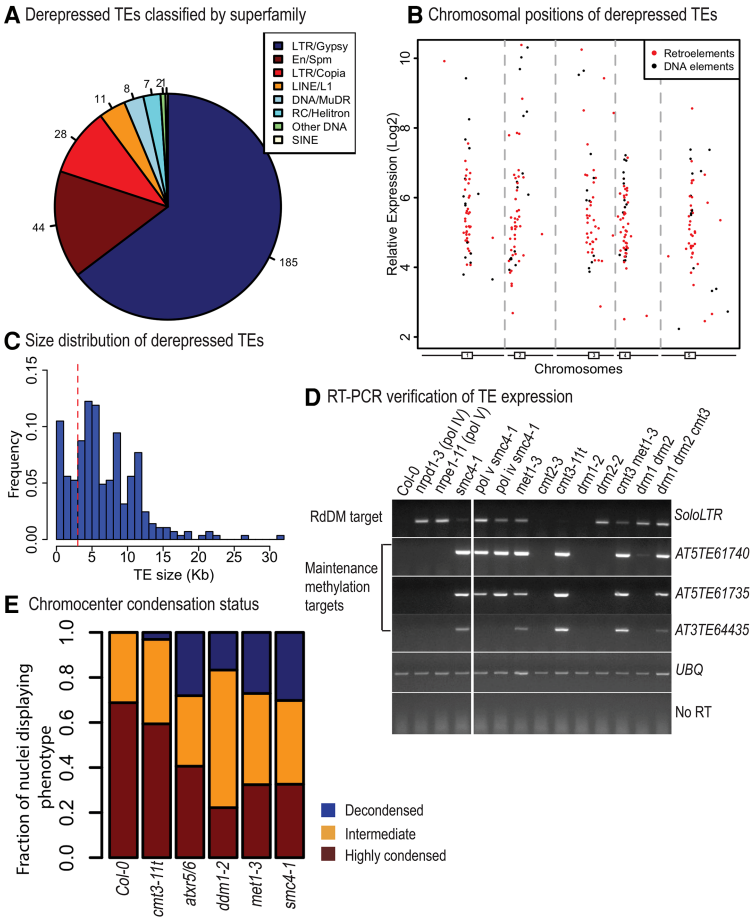

Figure 3. TEs in pericentromeric regions are derepressed in *smc4-1* mutants. (*A*) TEs derepressed at least fourfold in *smc4-1* (*smc4*/wild-type value of $\log_2 > 2$, with a false discovery rate [FDR] of ≤0.05). The 286 TEs are classified by superfamily. (*B*) Chromosomal positions of TEs derepressed fourfold or more in *smc4-1*. Retrotransposons are denoted by red dots, and DNA elements are denoted by black dots. Estimated centromere positions are shown for chromosomes 1–5 (from *left* to *right*), whose centromeres are represented by rectangles. (*C*) Size distribution of the 286 SMC4-repressed TEs. The *X*-axis shows the annotated TE size in kilobases, and the *Y*-axis shows the relative frequency of elements in each size class. The dashed red line marks 3 kb, beyond which TEs are classified as "long." (*D*) Overlap between TEs repressed by SMC4 and TEs repressed by maintenance cytosine methylation. Expression of three TEs derepressed in *smc4-1* (*AT5TE61740*, *AT5TE61735*, and *AT3TE64435*) and *soloLTR* (a target of RdDM) assayed by RT–PCR in mutants representing the RdDM pathway (*nrpd1*, *nrpe1*, *drm1-2*, and *drm2-2*), CG or CHG maintenance methylation pathways (*met1-3*, *cmt2-3*, and *cmt3-11t*), or the CHH maintenance methylation pathway (*cmt2-3*). *UBQ* and reactions from which reverse transcriptase was omitted (no RT) served as controls. (*E*) Relative frequencies of decondensed, partially decondensed (intermediate), or wild-type chromocenters in DAPI-stained nuclei of *cmt3-11t*, *atxr5/6*, *ddm1-2*, *met1-3*, *smc4-1*, or wild-type Col-0.

heterochromatic chromocenters become decondensed in *smc4-1* mutants as in *met1*, *cmt3*, or *ddm1* mutants (Fig. 3E; Supplemental Fig. S3; see also Soppe et al. 2002).

MET1, DDM1, H3K9 dimethylation (H3K9me2), H3K27 monomethylation (H3K27me1), and SMC4 silence overlapping subsets of TEs

To examine how transposons silenced by SMC4 overlap with transposons silenced by CG or CHG methylation, we compared *smc4-1* mRNA-seq data with published (Stroud et al. 2013) *met1*, *ddm1*, *cmt3*, or *suvh4/5/6* mRNA-seq data sets (Fig. 4). Two-thirds of all TEs derepressed fourfold or more in *met1* are also derepressed in *ddm1* mutants (636 of 956) (Fig. 4A), as reported previously (Stroud et al. 2013). Fewer TEs are derepressed in *smc4-1* (286) than in *met1* (956), but 63% (181 of 286) of these *SMC4*-dependent TEs overlap with TEs derepressed in *met1*, which is highly significant ($P = 3.60 \times 10^{-203}$) given an expectation of only 3.1% overlap by chance. It is important to note that *smc4-1* mutants are viable, whereas a *smc4* T-DNA insertion is lethal. Thus, the number of TEs up-regulated in *smc4-1* as a loss-of-function allele but not a null allele may underestimate the full effects of SMC4. Fifty-nine percent (169 of 286) of the TEs derepressed in *smc4-1* are derepressed in both *met1* and *ddm1* (Fig. 4A), which is also highly significant (*P* value of essentially 0) given an expected overlap (by chance) of only 0.08%.

In *cmt3-11* mutants, only 32 TEs are derepressed fourfold or more; however, 47% (15 of 32) of these overlap with TEs derepressed in *smc4-1* (Fig. 4B)—significantly more than the 0.92% expected by chance ($P = 9.27 \times 10^{-23}$). Moreover, 31% (10 of 32) of the TEs derepressed in *cmt3* overlap with TEs derepressed in *smc4-1*, *met1*, and *ddm1* (Fig. 4B,C)—significantly more than the 0.0007% expected by chance ($P = 1.99 \times 10^{-44}$).

Comparing *smc4-1* data with published *nrpe1* (*pol V*) mRNA-seq data (Blevins et al. 2014), only one derepressed TE was common to both data sets (Supplemental Fig. S4A), which is not statistically significant ($P = 0.25$). TEs derepressed in *smc4-1* also showed no further increase in expression in *smc4-1 nrpe1* or *smc4-1 nrpd1* double mutants (Supplemental Fig. S4B). Collectively, the results implicate condensin in MET1-, CMT3-, and DDM1-dependent transposon silencing but not silencing by RdDM.

Turning from DNA to histone methylation, 139 TEs are derepressed in a triple mutant for the H3K9 dimethylases *SUVH4*, *SUVH5*, and *SUVH6*. Of these TEs, 26.6% (37 of 139) are also derepressed in *smc4-1* (Fig. 4D), a

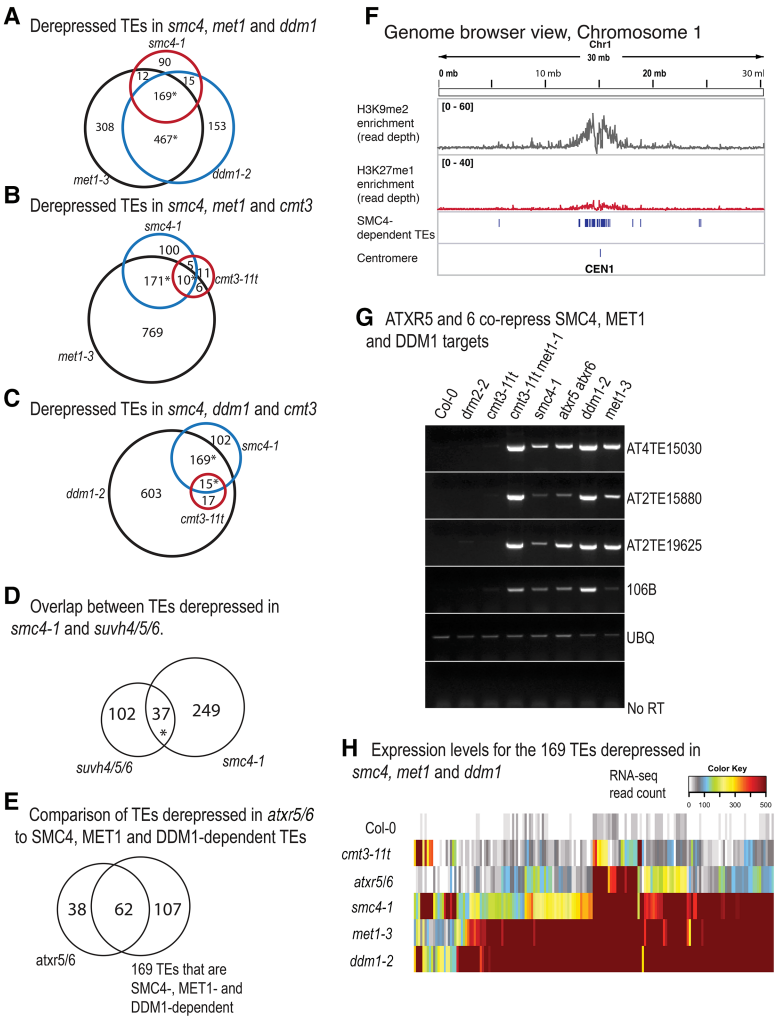

Figure 4. SMC4 coregulates loci silenced by maintenance DNA methylation and histone modifications associated with heterochromatin. (*A*) SMC4 silences a significant subset of MET1 and DDM1 targets. Venn diagram describing the relationship between TEs derepressed in the *smc4-1*, *met1-3*, and *ddm1-2* mutants. Asterisks denote statistically significant overlaps. (*B*) Venn diagram showing the overlap between TEs derepressed in the *smc4-1*, *met1-3*, and *cmt3-11t* mutants. Asterisks denote statistically significant overlaps. (*C*) Venn diagram describing the relationships between TEs derepressed in the *smc4-1*, *ddm1-2*, and *cmt3-11t* mutants. Asterisks denote statistically significant overlaps. (*D*) Overlap between TEs derepressed in *smc4-1* and *suvh4 suvh5 suvh6* triple mutants. Asterisks denote statistically significant overlaps. (*E*) ATXR5 and ATXR6 help silence a subset of TEs that also require MET1, DDM1, and SMC4. The Venn diagram compares the 100 TEs derepressed in an *atxr5 atxr6* double mutant with the 169 TEs that represent the overlap between the set of TEs derepressed in *met1*, *ddm1*, and *smc4-1*. (*F*) Genome browser snapshot of H3K9me2 enrichment, H3K27me1 enrichment, localization of SMC4-dependent TEs, and the centromeric position on chromosome 1 in wild-type Col-0. Raw counts of fragment pileup for the ChIP-seq (chromatin immunoprecipitation [ChIP] combined with high-throughput sequencing) data are shown in the *top* two tracks. Vertical bars in the third and fourth tracks represent SMC4-dependent TEs or centromeric repeats, respectively. (*G*) RT–PCR verification of the derepression of four TEs (*AT4TE15030*, *AT2TE15880*, *AT2TE19625*, and *106B*) predicted from RNA-seq data to be silenced via the partnership of MET1, DDM1, ATXR5/6, and SMC4. Genotypes tested are indicated at the *top* of the figure. *UBQ* reactions served as loading controls. Reactions omitting reverse transcriptase (no RT) control for DNA contamination. (*H*) Hierarchical clustering of the 169 TEs coregulated by SMC4, MET1, and DDM1, with TE expression levels displayed as a heat map. Expression levels were determined as RNA-seq reads corresponding to the TEs, normalized to the total number of mapped reads per genotype.

significant fraction ($P = 1.2 \times 10^{-43}$), indicating that a subset of TEs requires both H3K9me2 and SMC4 for silencing. Using the H3K9me2 ChIP-seq (chromatin immunoprecipitation [ChIP] combined with high-throughput sequencing) data of Stroud et al. (2014), we plotted the density of H3K9me2 (relative to total H3) at the 286 TEs derepressed in *smc4-1*, comparing these elements with a training set of 313 TEs randomly selected from the *Arabidopsis thaliana* genome (see Supplemental Tables S5, S6 for the lists of transposons examined). SMC4-dependent TEs show H3K9me2 enrichment throughout the elements in wild-type plants (Supplemental Fig. S5A) and lose this enrichment in *suvh4 suvh5 suvh6* triple mutants (Supplemental Fig. S5B). In contrast, the 313 randomly selected TEs show a lesser degree of H3K9me2 enrichment that is independent of *SUVH4/5/6*. Interestingly, genes whose repression involves SMC4 show no enrichment for H3K9me2 (Supplemental Fig. S5A,B), indicating that not all SMC4 targets are enriched for H3K9me2.

The H3K27 monomethylases ATXR5 and ATXR6 are functionally redundant paralogs important for the stability and silencing of pericentromeric heterochromatin (Jacob et al. 2009, 2010). TEs derepressed in *atxr5/6* double mutants show substantial overlap with TEs derepressed in *ddm1* or *met1* (Stroud et al. 2012). The H3K27me1 mark is enriched within the bodies of SMC4-dependent TEs as well as randomly selected TEs but not genes (Supplemental Fig. S5C). Therefore, we compared TEs derepressed fourfold or more in *atxr5/6* with the 169 TEs whose silencing is *SMC4*-, *MET1*-, and *DDM1*-dependent, revealing a 37% (62 of 169) overlap (Fig. 4E), which is significantly higher than the 0.32% expected by chance ($P = 4.34 \times 10^{-119}$).

Collectively, the overlap between H3K9me2, H3K27me1, and TEs repressed by SMC4 correlates with the enrichment of all three features in pericentromeric regions, as shown for chromosome 1 in Figure 4F.

As a test of the RNA-seq results, we examined the expression status of four TEs whose silencing is dependent

on *MET1*, *DDM1*, *SMC4*, and *ATXR5/6* using RT–PCR assays (Fig. 4G). This gel-based assay confirmed the conclusions from the RNA-seq data, showing that the TEs are silenced in wild-type plants (Col-0) but derepressed in each of the mutants.

Displaying RNA-seq data as a heat map, we compared the relative expression levels of the 169 *SMC4*-, *MET1*-, and *DDM1*-dependent TEs in *cmt3*, *atxr5/6*, *smc4*, *met1*, or *ddm1* mutants (Fig. 4H). *DDM1* and *MET1* exert the strongest repression of the largest number of TEs, with *SMC4* also needed for moderate to strong repression in most cases. *ATXR5* and *ATXR6* exert a less pronounced effect on TE expression, but a subset of TEs requires *SMC4*, *MET1*, *DDM1*, and *ATXR5/6* for strong repression.

DNA methylation and siRNA accumulation are unaltered in smc4-1 *mutants*

Because SMC4/condensin partners with cytosine methylation proteins in TE repression, we conducted genome-wide bisulfite sequencing to test whether SMC4 is required for DNA methylation. Transposons that are derepressed in *smc4-1* mutants are heavily methylated in all sequence contexts, as shown in the heat maps of Figure 5A. Their CG methylation is almost completely lost in *met1* mutants, their CHG methylation is greatly diminished in *cmt3* mutants, and their CHH methylation is depleted in *cmt2* mutants (Fig. 5A). Methylation in all three of these sequence contexts is also substantially reduced in *ddm1* mutants but not in *drm1 drm2* or *nrpe1* (*pol V*) mutants, consistent with maintenance methylation rather than RdDM. Importantly, DNA methylation is not appreciably affected in any sequence context in *smc4-1* mutants either at TEs regulated by *SMC4* (Fig. 5A) or genome-wide (Supplemental Fig. S6A). This is also apparent upon examining methylation patterns at individual loci, as shown for three TE loci in Figure 5B.

Recall that transgene-induced 21-nt siRNAs matching the *NRPE1* CTD region in the *cmt3 CTD-OX* line were absent in the m73 mutant. This led us to conduct small RNA deep sequencing (small RNA-seq) to see whether small RNA levels are affected by *smc4-1* genome-wide. We detected no change in siRNA levels relative to wild-type Col-0 in the *smc4-1* mutant for either 21- or 24-nt siRNAs (Fig. 5C; Supplemental Fig. S6B,C). This suggests that condensin somehow affects the *CTD-OX* transgene in a locus-specific manner without having genome-wide effects on 21-nt siRNA biogenesis.

MORC ATPases are thought to function downstream from DNA methylation to affect heterochromatin

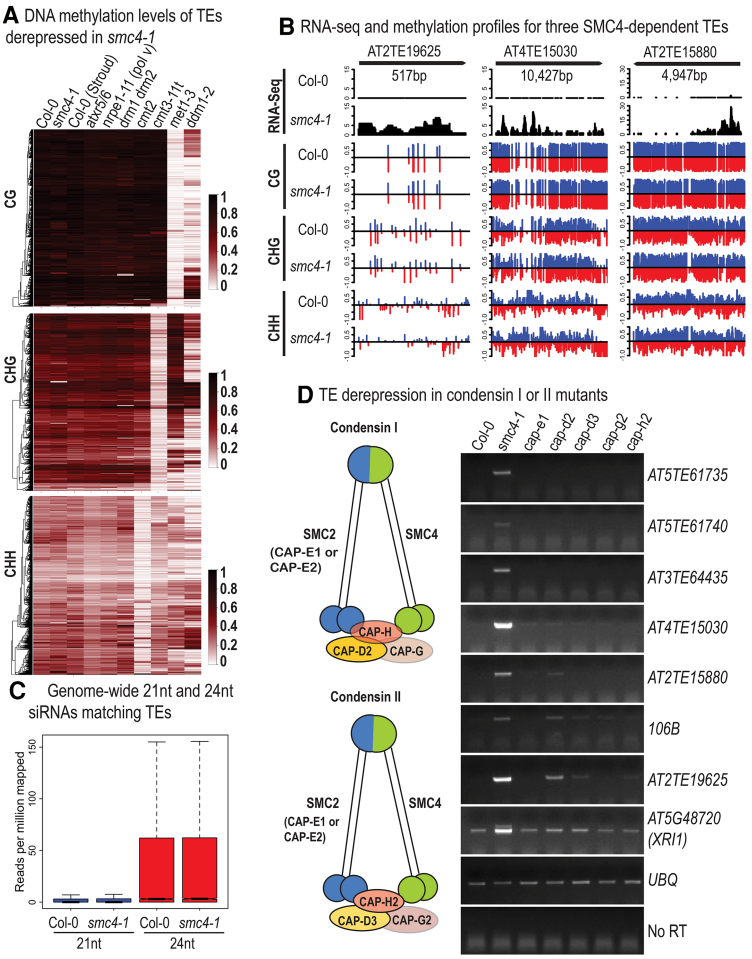

Figure 5. SMC4 does not affect cytosine methylation or siRNA levels and acts in the context of both condensins I and II. (*A*) Hierarchical clustering of the 286 SMC4-dependent TEs displaying DNA methylation levels on a scale of 0.0 (white) to 1.0 (black) in *smc4-1*, *atxr5/6*, *nrpe1* (*pol V*), *drm1 drm2*, *cmt2*, *cmt3*, *met1*, and *ddm1* mutants. Col-0 was the control from our study, and Col-0 (Stroud) was the control for the mutant methylome data of Stroud et al. (2012). Columns represent data for each indicated genotype, and rows represent 200-base-pair (bp) windows covering the 286 TEs. The rows were clustered by complete agglomeration hierarchical clustering method, with Euclidean distance as a distance measure. (*B*) RNA-seq and methylation profiles for three TEs (*AT2TE19625*, *AT4TE15030*, and *AT2TE15880*) cooperatively regulated by SMC4, MET1, DDM1, and ATXR5/6. The first two data tracks show mapped RNA-seq reads (black vertical bars) in the wild-type Col-0 and *smc4-1* mutant. The remaining six data tracks show cytosine methylation levels in each of the three sequence contexts (CG, CHG, and CHH). Methylation on the plus strand is plotted with blue vertical bars, and methylation on the minus strand is plotted with red vertical bars. TEs (black bars) are shown *above* the data tracks. (*C*) Box plot analyses comparing wild-type Col-0 and *smc4-1* with respect to 21- and 24-nt small RNA abundance genome-wide. All read counts were normalized to total mapped reads. (*D*) Involvement of condensins I and II in SMC4-dependent silencing. The cartoons at the *left* show the subunit compositions of *A. thaliana* condensins I and II. The gel images show RT–PCR results for SMC4-dependent loci, tested in the indicated condensin subunit mutants.

condensation (Jacob and Martienssen 2012; Lorkovic et al. 2012; Moissiard et al. 2012), possibly in ways similar to SMC ATPases (Iyer et al. 2008). Analyzing mRNA-seq data for *atmorc1 atmorc6* double mutants (Moissiard et al. 2012; Stroud et al. 2013), we found that 59% (26 of 44) of the TEs derepressed in *atmorc1/6* overlap with TEs derepressed in *met1* and *ddm1* (Supplemental Fig. S7A), which is significantly higher than the 0.08% expected by chance ($P = 1.07 \times 10^{-69}$) and comparable with the 59% overlap between TEs derepressed in *smc4-1*, *met1*, and *ddm*. Of the TEs derepressed in *atmorc1/6*, 41% (18 of 44) overlap with TEs derepressed in *smc4-1* (Supplemental Fig. S7B).

Collectively, our results indicate that TEs silenced in an *SMC4*-dependent manner are subject to multiple levels of control, including cytosine hypermethylation, histone H3K9me and H3K27me, and assembly into higher-order complexes that also involve MORC ATPases.

Both condensins I and II are involved in SMC4-dependent transposon silencing

SMC4 is a core subunit of condensin I and condensin II, making it unclear whether defective TE silencing in *smc4-1* stems from impairment of one or both forms of condensin. To address this question, we identified and tested homozygous T-DNA insertion mutants disrupting additional condensin subunits (Fig. 5D). These included CAP-E1, which is one of two SMC2 paralogs potentially present in either (or both) forms of condensin; CAP-D2, which is specific for condensin I; and the condensin II-specific subunits CAP-D3, CAP-G2, and CAP-H2. RT–PCR assays for expression of seven SMC4-dependent TEs demonstrated that all are derepressed to the greatest extent in *smc4-1* (Fig. 5D). In three cases (AT2TE15880, 106B, and AT2TE19625), condensin I appears to play the largest role, based on the level of TE expression in the *cap-d2* mutant, but condensin II subunit mutants also display some degree of TE derepression, indicating that both condensins I and II are important for silencing these elements. At the other four TEs, single mutants affecting condensin I- or II-specific subunits have little effect, suggesting that condensins I and II are redundant for silencing such that only mutations affecting both (*smc4-1*) bring about their derepression. No significant TE derepression was observed for the *cap-e1* mutant, suggesting that the CAP-E1 and CAP-E2 paralogs may be functionally redundant forms of SMC2.

SMC4/condensin represses sparsely methylated protein-coding genes

In addition to derepression of TEs, 533 protein-coding genes are significantly up-regulated in *smc4-1* mutants ($P < 0.01$; false discovery rate [FDR] < 0.05) (Supplemental Table S2). Unlike the TEs, which are mostly pericentromeric, the derepressed protein-coding genes are distributed throughout the chromosome arms (Fig. 6A). Also unlike the TEs, protein-coding genes regulated by SMC4 are only sparsely methylated (Fig. 6B).

Interestingly, 500 of the 533 up-regulated protein genes affect three major processes; namely, flower development, reproductive processes, and DNA repair (Fig. 6C; Supplemental Table S3). Up-regulation of four of the identified DNA repair genes (*GMI1*, *BRCA1*, *XRI1*, and *RAD51*) was verified by RT–PCR (Fig. 6D), consistent with a prior study that showed up-regulation of DNA repair genes in *Arabidopsis* mutants defective for two subunits specific to condensin II (Sakamoto et al. 2011). Moreover, *smc4-1* nuclei display prominent RAD51 repair foci (Fig. 6E), as in *atxr5/6* nuclei in which DNA damage is known to occur (Feng et al. 2017).

A flowering gene found by RNA-seq to be dramatically up-regulated in *smc4-1* mutants is *FLOWERING LOCUS T* (*FT*), which we verified using both gel-based RT–PCR assays (Fig. 6D) and qPCR (Fig. 7A). This likely explains the speedier transition to flowering observed under long-day conditions (16 h light, 8 h dark) for the original m73 mutant (genotype: *smc4-1 CTD-OX cmt3*) as well as the *smc4-1* line resulting from repeated backcrossing to wild-type Col-0 (Fig. 7B,C).

Another important gene regulated by SMC4 is *ROS1*, which encodes a DNA glycosylase that facilitates the removal and replacement of methylated cytosines by DNA repair (Gong et al. 2002). *ROS1* is up-regulated approximately fivefold in *smc4-1* (Fig. 7D), indicating that condensin limits the basal expression level of *ROS1*. Consistent with previous studies (He et al. 2009; Lei et al. 2015), *ROS1* expression is dependent on RdDM such that ROS1 expression is reduced in *nrpd1* (*pol IV*) *smc4-1* or *nrpe1* (*pol V*) *smc4-1* double mutants relative to the *smc4-1* single mutant (Fig. 7D) yet still remains higher than in a *pol V* single mutant. *ROS1* transcription levels positively correlate with RdDM-dependent methylation levels within a TE near the gene promoter (Lei et al. 2015; Williams et al. 2015). We observed a modest gain of methylation in all sequence contexts at this TE in the *smc4-1* mutant (Supplemental Fig. S8). Condensin may thus limit the extent of RdDM at this site in wild-type plants.

Discussion

Previous case studies have documented roles for condensin in repressing specific loci. For instance, in budding yeast, condensin helps repress silent mating type loci and also represses Pol II transcription within the intergenic spacers of Pol I transcribed ribosomal RNA genes (Bhalla et al. 2002; Machin et al. 2004; He et al. 2016). Consistent with the latter studies, the non-SMC condensin subunit AtCAP-H2 of *Arabidopsis* localizes within the nucleolus (Fujimoto et al. 2005), and rRNA genes become decondensed in *Arabidopsis* RNAi lines with reduced SMC4 levels (Smith et al. 2014). In flies, condensin is involved in position effect variegation (Lupo et al. 2001; Dej et al. 2004). In *C. elegans*, a specialized condensin is involved in X-chromosome dosage control (Meyer 2010), and, in mice, condensin helps maintain T-cell quiescence (Rawlings et al. 2011). Our results extend these case

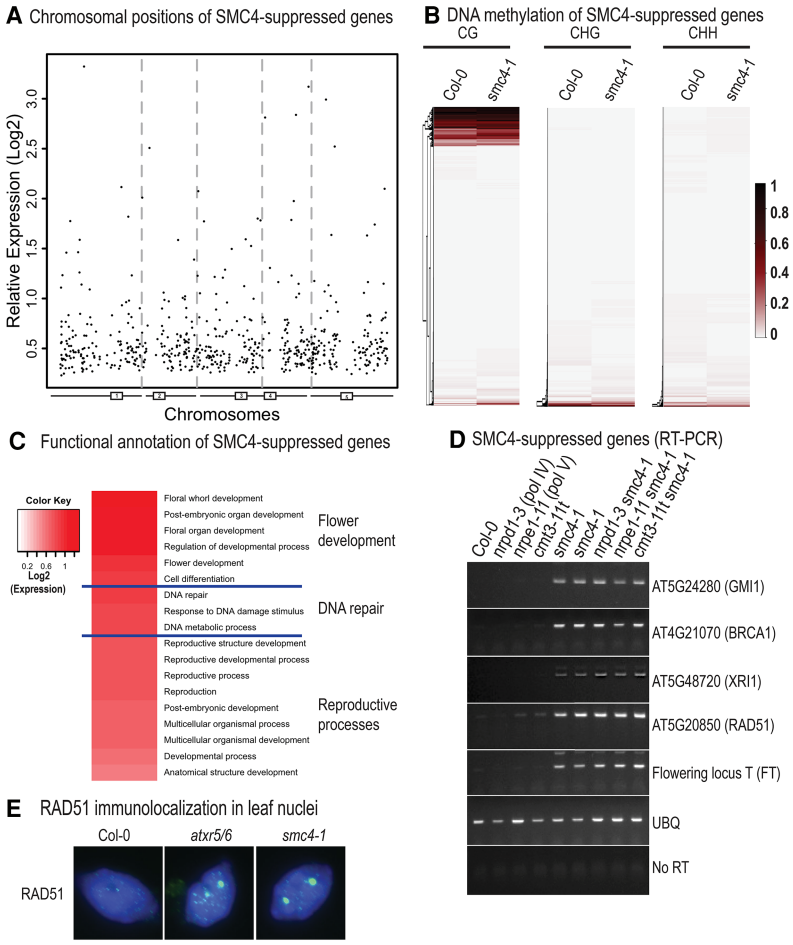

Figure 6. SMC4 represses protein-coding genes in addition to TEs. (*A*) Chromosomal positions and expression levels for protein-coding genes up-regulated in *smc4-1*. Estimated positions of centromeres are shown as boxes numbered accordingly for the five chromosomes. (*B*) Hierarchical clustering of the 533 SMC4-dependent protein-coding genes, displaying their relative DNA methylation levels on a scale of 0.0 (white) to 1.0 (red) in wild type and *smc4-1* mutants. Columns represent data for each indicated genotype, and rows represent 200-bp windows covering the 533 genes. The rows were clustered by the complete agglomeration hierarchical clustering method, with Euclidean distance as a distance measure. (*C*) Functional annotation of genes up-regulated in *smc4-1*. The color gradient reflects the degree of up-regulation in *smc4-1* relative to wild type on a $\log_2$ scale. (*D*) RT–PCR analysis of four DNA repair genes (*GMI1*, *BRCA1*, *XRI1*, and *RAD51*) and the flowering gene *Flowering Locus T* (*FT*) predicted by RNA-seq to be up-regulated in *smc4-1*. *UBQ* and no reverse transcriptase (no RT) reactions served as controls. (*E*) *smc4-1* nuclei display RAD51 enrichment foci indicative of DNA damage, consistent with the up-regulation of DNA repair genes. Images show immunolocalization of RAD51 in leaf nuclei counterstained with DAPI. The *atxr5 atxr6* mutant, known to cause genome instability (Feng et al. 2017), served as a positive control for enhanced RAD51 foci.

studies to a whole-genome level, made possible by the identification of *smc4-1* as a viable, yet deleterious, mutation of the essential *SMC4* gene. Our findings indicate that condensin acts as a corepressor of both genes and transposons, affecting hundreds of loci.

Our results indicate that condensin partners with symmetrical cytosine methylation and repressive histone modifications, particularly ATXR5/6-dependent H3K27me1, in the repression of pericentromeric transposons. MET1 and ATXR5/6 are thought to be recruited to DNA replication forks by interacting with PCNA (Chuang et al. 1997; Raynaud et al. 2006; Hale et al. 2016). Interestingly, condensin has been detected at stalled DNA replication forks (D'Ambrosio et al. 2008) and shown to interact with DNA methyltransferases in mammalian cells (Geiman et al. 2004). These observations suggest that compact repressive chromatin structures might assemble quickly following DNA replication.

Condensin is needed for *Drosophila* Gypsy family retrotransposons to cluster within distinct chromatin bodies (Gerasimova et al. 2000) and for LTR retroelements in *Schizosaccharomyces pombe* to cluster in the vicinity of centromeres (Cam et al. 2008; Tanaka et al. 2012; Murton et al. 2016). How are these dispersed elements recognized and brought together? The fact that *Arabidopsis* loci that are heavily cytosine methylated or sparsely methylated can be regulated by condensin argues against DNA methylation as a primary determinant of condensin recruitment, as does the fact that flies and yeast do not appreciably methylate their DNA. Conserved histone modifications or histone variants present in all eukaryotes seem more likely as marks that enable condensin recruitment. Architectural chromatin proteins such as heterochromatin protein 1 (HP1) family members, Polycomb-repressive complex 1 (PRC1) family proteins, or yeast silent information regulator (SIR) proteins might then serve as intermediaries for condensin recruitment (McBryant et al. 2006; Woodcock and Ghosh 2010; Grossniklaus and Paro 2014).

The mutation in the *smc4-1* allele P22S is intriguing in that the substituted proline is highly conserved except in budding yeast, which has a serine at this position, as in *smc4-1* (see Fig. 2D). It is plausible that the P-to-S mutation might be tolerated as a hypomorphic mutant in other model organisms, including mammals, in which null mutants are lethal. Given that somatic mutations in condensin subunits occur in multiple types of cancer (Leiserson et al. 2015; Uhlmann 2016), generating this mutation by gene editing might prove useful for genome-wide identification of loci that become derepressed in human cells when condensin function is compromised.

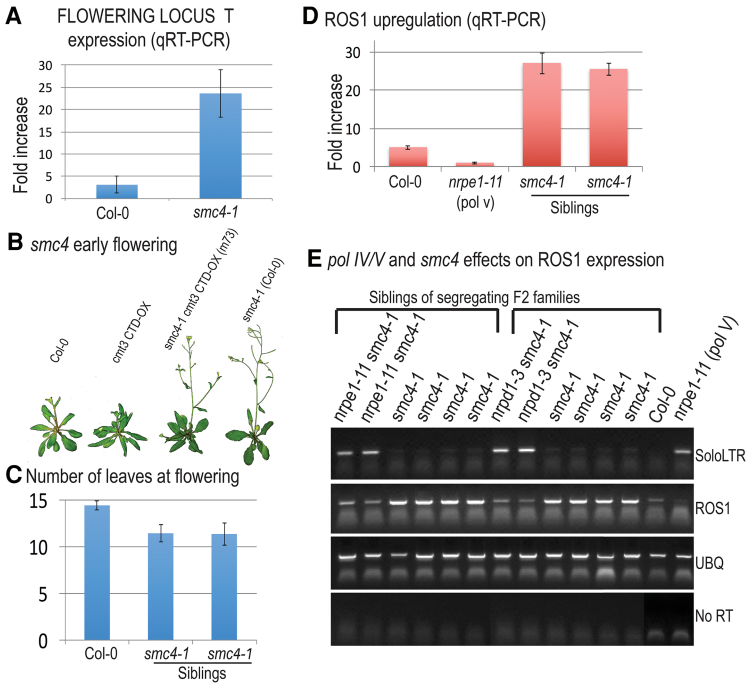

Figure 7. Early flowering and up-regulation of the ROS1 demethylase in *smc4-1*. (*A*) Early flowering of *smc4-1* correlates with the up-regulation of *FT* expression. The histogram shows qRT–PCR results for *FT* expression relative to *ACTIN* using RNA of pooled wild-type Col-0 or *smc4-1* plants. Error bars indicate the standard deviation in three independent technical replicates. (*B*) *smc4-1* mutants flower early. The images show 3-wk-old plants grown under long-day (16 h light) conditions, comparing wild type (Col-0), *cmt3 CTD-OX*, m73 (the *smc4-1* mutation in the *cmt3 CTD-OX* background), and *smc4-1* in an otherwise wild-type Col-0 background. (*C*) Quantification of the number of vegetative leaves present at the time of flowering. The histograms show mean values and standard deviations (error bars) determined for 18 Col-0, 19 *smc4-1* (Col-0), or 18 *smc4-1* (Col-0) plants. The two sets of *smc4-1* plants represent independent families derived from F2 siblings resulting from the second round of Col-0 X *smc4-1* backcrossing. (*D*) qRT–PCR analysis of *ROS1* expression in wild type, *nrpe1-11* (*pol V*), and *smc4-1* mutants. The two *smc4-1* samples represent siblings of the F2 family resulting from the second round of Col-0 X *smc4-1* backcrossing. The data were normalized to *ACTIN*, with error bars indicating standard deviations based on three independent technical replicates. (*E*) RT–PCR analysis of *ROS1* gene expression in *smc4-1*, *nrpd1-3* (*pol IV*) *smc4-1*, and *nrpe1-11* (*pol V*) *smc4-1* mutants. *SoloLTR* served as a control for the Pol IV- and Pol V-dependent RdDM effect. *UBQ* and no reverse transcriptase (no RT) reactions served as controls.

Materials and methods

Plant materials

A. thaliana ecotype Col-0 was used in all experiments. *met1-3* and *ddm1-2* were described in Saze et al. (2003), and *nrpd1-3* (*pol IV*) and *nrpe1-11* (*pol V*) mutants were described previously (Onodera et al. 2005; Pontes et al. 2006). *atxr5 atxr6* was provided by Scott Michaels, and *met1-1* was provided by Eric Richards. *drm2-2* and *cmt3-11t* were obtained from the *Arabidopsis* Biological Resource Center (ABRC). The *cmt3-11t met1-1* double mutant was created by crossing *cmt3-11t* to *met1-1* (Pontvianne et al. 2013). The *SMC4* T-DNA insertion mutant line SAIL-86-D02 (Siddiqui et al. 2006) was obtained from the ABRC. Mutant lines of the condensin subunits *cap-e1* (CS84719), *cap-d2* (SALK_077796C), *cap-d3* (SALK_094776), *cap-g2* (SALK-049790C), and *cap-h2* (SALK_059304) were obtained from the ABRC.

The *CTD-OX* transgene corresponding to NRPE1 sequences encoding amino acids 1249–1976 was cloned into pEarleyGate 202 (Earley et al. 2006) and then transformed into *cmt3-11t* by the floral dip method (Clough and Bent 1998). Transgenic plants were selected by Basta herbicide resistance, and 431 positive transformants were further screened to identify 242 lines with Basta resistance, segregating 3:1. These 242 lines were next subjected to Southern blot analysis to identify plants with single T-DNA left and right border fragments. Line #389 (*cmt3 OX-CTD*) was chosen for EMS mutagenesis. An *OX-CTD* line was obtained by backcrossing #389 (*cmt3 OX-CTD*) to Col-0 and identifying F2 individuals lacking *cmt3* mutant alleles.

EMS mutagenesis and genetic mapping

Approximately 22,000 *cmt3 CTD-OX* line seeds were mutagenized with EMS as described (Kim et al. 2006), except that the EMS concentration was 0.3%. Seeds of resulting M1 plants were harvested, and resulting M2 plants with a wild-type (as opposed to SDC) phenotype were identified. Bulked-segregant analysis and sequence-based mapping were conducted as described by Hartwig et al. (2012). Briefly, putative suppressor mutants were first backcrossed to the *cmt3 CTD-OX* parental line, and resulting F1 plants were grown and allowed to self-pollinate to produce F2 seeds. F2 plants were then grown, and 50 plants displaying SDC or wild-type phenotypes were pooled, and their DNA was subjected to library construction and deep sequencing, with an estimated genome coverage of 30×. The *cmt3 CTD-OX* line was also sequenced. Candidate EMS-induced mutations absent in the parental line and displaying high allele frequencies in suppressor mutants were confirmed by sequencing of PCR-amplified genomic DNA.

Complementation of smc4-1 *by an* SMC4 *transgene*

Plant transformation vector pHPT carrying a full-length wild-type *SMC4* genomic clone insert (Siddiqui et al. 2006) was provided by Daniel Riggs. The plasmid was transformed into *Agrobacterium tumefaciens* strain GV3101 and subsequently used to transform *smc4-1* mutant plants. Transformants were initially selected by hygromycin resistance and verified using PCR assays.

DNA genotyping analyses

For T-DNA mutant genotyping, genomic DNA from 2-wk-old plants was isolated using CTAB extraction. GoTaq Green master mix (2×; Promega) was mixed with ~100 ng of genomic DNA and appropriate primer pairs. PCR products were resolved and visualized by agarose gel electrophoresis. Genotyping primers are listed in Supplemental Table S4. Genotyping of *smc4-1* involved PCR amplification followed by HindIII digestion; the *smc4-1* mutant was cleaved, whereas the wild-type gene was not.

DNA methylation analyses

Genomic DNA was isolated from 2-wk-old plants using the Nucleon PhytoPure DNA extraction kit (Amersham). Chop-PCR assays were performed using 100 ng of restriction endonuclease-digested ("chopped") genomic DNA as in Blevins et al. (2017). Bisulfite sequencing analysis of the *ROS1* promoter regions was according to Blevins et al. (2014). In brief, PCR fragments amplified from bisulfite-treated DNA were cloned into pGEM-T-Easy and sequenced using a T7 primer. Forty-eight sequences per amplicon were analyzed in CyMATE (Hetzl et al. 2007). Chop-PCR and bisulfite sequencing primers are listed in Supplemental Table S4.

Semiquantitative RT–PCR

Total RNA was extracted from three to four leaves of 2-wk-old plants using the Spectrum plant total RNA kit (Sigma-Aldrich). RNA (1.5 µg) was then treated using a Turbo DNA-free kit (Thermo Fisher Scientific) and used for random-primed cDNA synthesis using SuperScript III reverse transcriptase (Invitrogen). Resulting cDNA was used for PCR amplification using GoTaq Green polymerase (Promega) and primers listed in Supplemental Table S4.

RNA-seq and data analysis

Total RNA was extracted from 2-wk-old *Arabidopsis* leaves using TRI reagent (MRC, Inc.). Libraries for three biological replicates of each genotype were constructed and sequenced using the Illumina NextSeq 500 platform. TrueSeq adaptor sequences were trimmed using Trimmomatic version 0.33. Reads post-trimming were filtered with a quality score cutoff of 20 and length cutoff of 30. Filtered reads were mapped to the TAIR10 genome using TopHat 2.0.10. The number of uniquely mapped reads corresponding to annotated protein-coding genes or TEs were computed using HTSeq-count version 0.5.4p1 (Anders et al. 2015). The DESeq2 package in R (Love et al. 2014) was used for calling significantly differentially expressed genes and TEs. Differentially expressed genes were defined as those with <5% FDR and a *P*-value cutoff of 0.01, whereas derepressed TEs were defined as those with a <5% FDR and a fold change in log base 2 of >2. The identification and evaluation of statistical significance for intersections among multiple sets of derepressed TEs were conducted using the "SuperExactTest" package in R (Wang et al. 2015).

Whole-genome bisulfite sequencing and data analysis

Genomic DNA was isolated from 2-wk-old *Arabidopsis* leaves using an Illustra Nucleon PhytoPure DNA extraction kit (GE Healthcare). Three biological replicates of each genotype were submitted to the Beijing Genome Institute (http://www.genomics.cn/en) for bisulfite treatment, library preparation, and Illumina sequencing. For data analysis, adapters were trimmed, low-quality sequences ($q < 20$) were filtered, and clean reads were mapped to the TAIR10 genome using Bismark (Krueger and Andrews 2011). Methylated cytosines supported by at least five reads were passed to the MethylKit package in R for further analysis (Akalin et al. 2012). For calling differentially methylated cytosines in CG, CHG, and CHH contexts, threshold differences of at least 50%, 25%, and 15% methylation, respectively, were required along with *P*-values of <0.01. Differentially methylated regions were defined as regions containing at least 10 differentially methylated cytosines in each 200-base-pair (bp) sliding window, with a step size of 150 bp. DNA methylation levels were compared between each wild-type and mutant window using Fisher's exact test with a *P*-value cutoff of 0.05. The *P*-values were adjusted using the standard Benjamini-Hochberg method to control for FDRs.

Small RNA-seq and blot analyses

Total RNA was extracted from 2-wk-old *Arabidopsis* seedlings using TRIzol (ThermoFisher Scientific) and submitted to Fasteris SA (http://www.fasteris.com) for library construction and small RNA-seq, performed on an Illumina HiSeq 2000 platform. RNA size fractionation was conducted as in Blevins et al. (2014) except that gel slices containing RNAs of 15–30 nt were used rather than RNAs of 15–45 nt. For small RNAs, reads were first adaptor-trimmed to remove TruSeq 3′ small RNA adaptor sequences using Trimmomatic version 0.33 (Bolger et al. 2014) and then quality-trimmed, setting the cutoff threshold for average base quality score at 20 over a window of 3 bases. Reads >15 bases post-trimming were excluded. Trimmed and filtered reads were then mapped to the TAIR10 reference genome sequence using Bowtie version 1.1.2 (Langmead et al. 2009), and only perfectly matched 21- to 25-nt RNAs were analyzed further. Any reads aligning to 45S rRNA, chloroplast, or mitochondria were excluded. Read alignments were further filtered for size classes 21 and 24 nt.

For small RNA Northern blot analyses, ~100 µg of total RNA was extracted from 2-wk-old seedlings using TRIzol (ThermoFisher Scientific) and then size-fractionated on RNeasy minicolumns (Qiagen) (Blevins et al. 2006). The low-molecular-weight RNA fraction was then used as described previously (Blevins et al. 2015).

Accession numbers

Sequence data generated in this study have been deposited in the NCBI Sequence Read Archive (http://www.ncbi.nlm.nih.gov/sra) under accession number SRP105760.

Acknowledgments

We thank Dan Riggs for providing the *SMC4* genomic clone, James Ford and the Indiana University (IU) Center for Genomics and Bioinformatics, and Jim Powers and the IU Light Microscopy Imaging Center. This work was supported by funds made available to C.S.P. by National Institutes of Health grant GM077590 and Gordon and Betty Moore Foundation grant 3036 and funds made available to C.S.P. as an Investigator of the Howard Hughes Medical Institute. T.B. and E.H.T. generated the *cmt3 CTD-OX* line that provided the basis for the genetic screen, based on initial experiments by J.R.H., who engineered the CTD-OX transgene and identified the dominant-negative *nrpe1* phenotype that it induces. J.W. and T.B. developed the bioinformatics pipeline for mapping EMS-generated point mutations. J.W. and R.P. performed all bioinformatics except those for Figure 4F and Supplemental Figure S5, conducted by F.W. J.W. conducted all remaining experiments. J.W. and C.S.P. wrote the manuscript.

References

Akalin A, Kormaksson M, Li S, Garrett-Bakelman FE, Figueroa ME, Melnick A, Mason CE. 2012. methylKit: a comprehensive R package for the analysis of genome-wide DNA methylation profiles. *Genome Biol* **13:** R87.

Allen E, Xie Z, Gustafson AM, Carrington JC. 2005. microRNA-directed phasing during *trans*-acting siRNA biogenesis in plants. *Cell* **121:** 207–221.

Anders S, Pyl PT, Huber W. 2015. HTSeq—a Python framework to work with high-throughput sequencing data. *Bioinformatics* **31:** 166–169.

Bhalla N, Biggins S, Murray AW. 2002. Mutation of YCS4, a budding yeast condensin subunit, affects mitotic and nonmitotic chromosome behavior. *Mol Biol Cell* **13:** 632–645.

Blevins T, Rajeswaran R, Shivaprasad PV, Beknazariants D, Si-Ammour A, Park HS, Vazquez F, Robertson D, Meins F Jr, Hohn T, et al. 2006. Four plant Dicers mediate viral small RNA biogenesis and DNA virus induced silencing. *Nucleic Acids Res* **34:** 6233–6246.

Blevins T, Pontvianne F, Cocklin R, Podicheti R, Chandrasekhara C, Yerneni S, Braun C, Lee B, Rusch D, Mockaitis K, et al. 2014. A two-step process for epigenetic inheritance in *Arabidopsis*. *Mol Cell* **54:** 30–42.

Blevins T, Podicheti R, Mishra V, Marasco M, Wang J, Rusch D, Tang H, Pikaard CS. 2015. Identification of Pol IV and RDR2-dependent precursors of 24 nt siRNAs guiding de novo DNA methylation in *Arabidopsis*. *Elife* **4:** e09591.

Blevins T, Wang J, Pflieger D, Pontvianne F, Pikaard CS. 2017. Hybrid incompatibility caused by an epiallele. *Proc Natl Acad Sci* **114:** 3702–3707.

Bolger AM, Lohse M, Usadel B. 2014. Trimmomatic: a flexible trimmer for Illumina sequence data. *Bioinformatics* **30:** 2114–2120.

Bostick M, Kim JK, Esteve PO, Clark A, Pradhan S, Jacobsen SE. 2007. UHRF1 plays a role in maintaining DNA methylation in mammalian cells. *Science* **317:** 1760–1764.

Brzeski J, Jerzmanowski A. 2003. Deficient in DNA methylation 1 (DDM1) defines a novel family of chromatin-remodeling factors. *J Biol Chem* **278:** 823–828.

Cam HP, Noma K, Ebina H, Levin HL, Grewal SI. 2008. Host genome surveillance for retrotransposons by transposon-derived proteins. *Nature* **451:** 431–436.

Cao X, Jacobsen SE. 2002. Role of the *Arabidopsis* DRM methyltransferases in de novo DNA methylation and gene silencing. *Curr Biol* **12:** 1138–1144.

Cao X, Aufsatz W, Zilberman D, Mette MF, Huang MS, Matzke M, Jacobsen SE. 2003. Role of the DRM and CMT3 methyltransferases in RNA-directed DNA methylation. *Curr Biol* **13:** 2212–2217.

Chuang LS, Ian HI, Koh TW, Ng HH, Xu G, Li BF. 1997. Human DNA-(cytosine-5) methyltransferase-PCNA complex as a target for p21WAF1. *Science* **277:** 1996–2000.

Clough SJ, Bent AF. 1998. Floral dip: a simplified method for *Agrobacterium*-mediated transformation of *Arabidopsis thaliana*. *Plant J* **16:** 735–743.

D'Ambrosio C, Schmidt CK, Katou Y, Kelly G, Itoh T, Shirahige K, Uhlmann F. 2008. Identification of *cis*-acting sites for condensin loading onto budding yeast chromosomes. *Genes Dev* **22:** 2215–2227.

Dej KJ, Ahn C, Orr-Weaver TL. 2004. Mutations in the *Drosophila* condensin subunit dCAP-G: defining the role of condensin for chromosome condensation in mitosis and gene expression in interphase. *Genetics* **168:** 895–906.

Earley KW, Haag JR, Pontes O, Opper K, Juehne T, Song K, Pikaard CS. 2006. Gateway-compatible vectors for plant functional genomics and proteomics. *Plant J* **45:** 616–629.

Feng W, Hale CJ, Over RS, Cokus SJ, Jacobsen SE, Michaels SD. 2017. Large-scale heterochromatin remodeling linked to overreplication-associated DNA damage. *Proc Natl Acad Sci* **114:** 406–411.

Fransz P, De Jong JH, Lysak M, Castiglione MR, Schubert I. 2002. Interphase chromosomes in *Arabidopsis* are organized as well defined chromocenters from which euchromatin loops emanate. *Proc Natl Acad Sci* **99:** 14584–14589.

Fujimoto S, Yonemura M, Matsunaga S, Nakagawa T, Uchiyama S, Fukui K. 2005. Characterization and dynamic analysis of *Arabidopsis* condensin subunits, AtCAP-H and AtCAP-H2. *Planta* **222:** 293–300.

Geiman TM, Sankpal UT, Robertson AK, Chen Y, Mazumdar M, Heale JT, Schmiesing JA, Kim W, Yokomori K, Zhao Y, et al. 2004. Isolation and characterization of a novel DNA methyltransferase complex linking DNMT3B with components of the mitotic chromosome condensation machinery. *Nucleic Acids Res* **32:** 2716–2729.

Gerasimova TI, Byrd K, Corces VG. 2000. A chromatin insulator determines the nuclear localization of DNA. *Mol Cell* **6:** 1025–1035.

Gong Z, Morales-Ruiz T, Ariza RR, Roldan-Arjona T, David L, Zhu JK. 2002. ROS1, a repressor of transcriptional gene silencing in *Arabidopsis*, encodes a DNA glycosylase/lyase. *Cell* **111:** 803–814.

Grossniklaus U, Paro R. 2014. Transcriptional silencing by polycomb-group proteins. *Cold Spring Harb Perspect Biol* **6:** a019331.

Haag JR, Pikaard CS. 2011. Multisubunit RNA polymerases IV and V: purveyors of non-coding RNA for plant gene silencing. *Nat Rev Mol Cell Biol* **12:** 483–492.

Hale CJ, Potok ME, Lopez J, Do T, Liu A, Gallego-Bartolome J, Michaels SD, Jacobsen SE. 2016. Identification of multiple proteins coupling transcriptional gene silencing to genome stability in *Arabidopsis thaliana*. *PLoS Genet* **12:** e1006092.

Hartwig B, James GV, Konrad K, Schneeberger K, Turck F. 2012. Fast isogenic mapping-by-sequencing of ethyl methanesulfonate-induced mutant bulks. *Plant Physiol* **160:** 591–600.

Hashimoto H, Horton JR, Zhang X, Bostick M, Jacobsen SE, Cheng X. 2008. The SRA domain of UHRF1 flips 5-methylcytosine out of the DNA helix. *Nature* **455:** 826–829.

He XJ, Hsu YF, Zhu S, Liu HL, Pontes O, Zhu J, Cui X, Wang CS, Zhu JK. 2009. A conserved transcriptional regulator is required for RNA-directed DNA methylation and plant development. *Genes Dev* **23:** 2717–2722.

He HJ, Zhang S, Wang D, Hochwagen A, Li F. 2016. Condensin promotes position effects within tandem DNA repeats via the RITS complex. *Cell Rep* **14:** 1018–1024.

Henderson IR, Jacobsen SE. 2008. Tandem repeats upstream of the *Arabidopsis* endogene SDC recruit non-CG DNA methylation and initiate siRNA spreading. *Genes Dev* **22:** 1597–1606.

Hetzl J, Foerster AM, Raidl G, Mittelsten Scheid O. 2007. CyMATE: a new tool for methylation analysis of plant genomic DNA after bisulphite sequencing. *Plant J* **51:** 526–536.

Hirano T. 2016. Condensin-based chromosome organization from bacteria to vertebrates. *Cell* **164:** 847–857.

Iyer LM, Anantharaman V, Wolf MY, Aravind L. 2008. Comparative genomics of transcription factors and chromatin proteins in parasitic protists and other eukaryotes. *Int J Parasitol* **38:** 1–31.

Jacob Y, Martienssen R. 2012. All packed up and ready to go. *Science* **336:** 1391–1392.

Jacob Y, Feng S, LeBlanc CA, Bernatavichute YV, Stroud H, Cokus S, Johnson LM, Pellegrini M, Jacobsen SE, Michaels SD. 2009. ATXR5 and ATXR6 are H3K27 monomethyltransferases required for chromatin structure and gene silencing. *Nat Struct Mol Biol* **16:** 763–768.

Jacob Y, Stroud H, Leblanc C, Feng S, Zhuo L, Caro E, Hassel C, Gutierrez C, Michaels SD, Jacobsen SE. 2010. Regulation of

heterochromatic DNA replication by histone H3 lysine 27 methyltransferases. *Nature* **466:** 987–991.

Jeddeloh JA, Stokes TL, Richards EJ. 1999. Maintenance of genomic methylation requires a SWI2/SNF2-like protein. *Nat Genet* **22:** 94–97.

Jeppsson K, Kanno T, Shirahige K, Sjogren C. 2014. The maintenance of chromosome structure: positioning and functioning of SMC complexes. *Nat Rev Mol Cell Biol* **15:** 601–614.

Kim Y, Schumaker KS, Zhu JK. 2006. EMS mutagenesis of *Arabidopsis*. *Methods Mol Biol* **323:** 101–103.

Krueger F, Andrews SR. 2011. Bismark: a flexible aligner and methylation caller for Bisulfite-Seq applications. *Bioinformatics* **27:** 1571–1572.

Langmead B, Trapnell C, Pop M, Salzberg SL. 2009. Ultrafast and memory-efficient alignment of short DNA sequences to the human genome. *Genome Biol* **10:** R25.

Law JA, Jacobsen SE. 2010. Establishing, maintaining and modifying DNA methylation patterns in plants and animals. *Nat Rev Genet* **11:** 204–220.

Lei M, Zhang H, Julian R, Tang K, Xie S, Zhu JK. 2015. Regulatory link between DNA methylation and active demethylation in *Arabidopsis*. *Proc Natl Acad Sci* **112:** 3553–3557.

Leiserson MD, Vandin F, Wu HT, Dobson JR, Eldridge JV, Thomas JL, Papoutsaki A, Kim Y, Niu B, McLellan M, et al. 2015. Pan-cancer network analysis identifies combinations of rare somatic mutations across pathways and protein complexes. *Nat Genet* **47:** 106–114.

Lippman Z, Gendrel AV, Black M, Vaughn MW, Dedhia N, McCombie WR, Lavine K, Mittal V, May B, Kasschau KD, et al. 2004. Role of transposable elements in heterochromatin and epigenetic control. *Nature* **430:** 471–476.

Lorkovic ZJ, Naumann U, Matzke AJ, Matzke M. 2012. Involvement of a GHKL ATPase in RNA-directed DNA methylation in *Arabidopsis thaliana*. *Curr Biol* **22:** 933–938.

Love MI, Huber W, Anders S. 2014. Moderated estimation of fold change and dispersion for RNA-seq data with DESeq2. *Genome Biol* **15:** 550.

Lupo R, Breiling A, Bianchi ME, Orlando V. 2001. Drosophila chromosome condensation proteins Topoisomerase II and Barren colocalize with Polycomb and maintain Fab-7 PRE silencing. *Mol Cell* **7:** 127–136.

Machin F, Paschos K, Jarmuz A, Torres-Rosell J, Pade C, Aragon L. 2004. Condensin regulates rDNA silencing by modulating nucleolar Sir2p. *Curr Biol* **14:** 125–130.

Mallory A, Vaucheret H. 2010. Form, function, and regulation of ARGONAUTE proteins. *Plant Cell* **22:** 3879–3889.

Matzke MA, Mosher RA. 2014. RNA-directed DNA methylation: an epigenetic pathway of increasing complexity. *Nat Rev Genet* **15:** 394–408.

McBryant SJ, Adams VH, Hansen JC. 2006. Chromatin architectural proteins. *Chromosome Res* **14:** 39–51.

Meyer BJ. 2010. Targeting X chromosomes for repression. *Curr Opin Genet Dev* **20:** 179–189.

Moissiard G, Cokus SJ, Cary J, Feng S, Billi AC, Stroud H, Husmann D, Zhan Y, Lajoie BR, McCord RP, et al. 2012. MORC family ATPases required for heterochromatin condensation and gene silencing. *Science* **336:** 1448–1451.

Mourrain P, Beclin C, Elmayan T, Feuerbach F, Godon C, Morel JB, Jouette D, Lacombe AM, Nikic S, Picault N, et al. 2000. *Arabidopsis* SGS2 and SGS3 genes are required for posttranscriptional gene silencing and natural virus resistance. *Cell* **101:** 533–542.

Murton HE, Grady PJ, Chan TH, Cam HP, Whitehall SK. 2016. Restriction of retrotransposon mobilization in *Schizosaccharomyces pombe* by transcriptional silencing and higher-order chromatin organization. *Genetics* **203:** 1669–1678.

Onodera Y, Haag JR, Ream T, Costa Nunes P, Pontes O, Pikaard CS. 2005. Plant nuclear RNA polymerase IV mediates siRNA and DNA methylation-dependent heterochromatin formation. *Cell* **120:** 613–622.

Peragine A, Yoshikawa M, Wu G, Albrecht HL, Poethig RS. 2004. SGS3 and SGS2/SDE1/RDR6 are required for juvenile development and the production of *trans*-acting siRNAs in *Arabidopsis*. *Genes Dev* **18:** 2368–2379.

Pontes O, Li CF, Costa Nunes P, Haag J, Ream T, Vitins A, Jacobsen SE, Pikaard CS. 2006. The *Arabidopsis* chromatin-modifying nuclear siRNA pathway involves a nucleolar RNA processing center. *Cell* **126:** 79–92.

Pontvianne F, Blevins T, Chandrasekhara C, Mozgova I, Hassel C, Pontes OM, Tucker S, Mokros P, Muchova V, Fajkus J, et al. 2013. Subnuclear partitioning of rRNA genes between the nucleolus and nucleoplasm reflects alternative epiallelic states. *Genes Dev* **27:** 1545–1550.

Rawlings JS, Gatzka M, Thomas PG, Ihle JN. 2011. Chromatin condensation via the condensin II complex is required for peripheral T-cell quiescence. *EMBO J* **30:** 263–276.

Raynaud C, Sozzani R, Glab N, Domenichini S, Perennes C, Cella R, Kondorosi E, Bergounioux C. 2006. Two cell-cycle regulated SET-domain proteins interact with proliferating cell nuclear antigen (PCNA) in *Arabidopsis*. *Plant J* **47:** 395–407.

Sakamoto T, Inui YT, Uraguchi S, Yoshizumi T, Matsunaga S, Mastui M, Umeda M, Fukui K, Fujiwara T. 2011. Condensin II alleviates DNA damage and is essential for tolerance of boron overload stress in *Arabidopsis*. *Plant Cell* **23:** 3533–3546.

Saze H, Mittelsten Scheid O, Paszkowski J. 2003. Maintenance of CpG methylation is essential for epigenetic inheritance during plant gametogenesis. *Nat Genet* **34:** 65–69.

Siddiqui NU, Rusyniak S, Hasenkampf CA, Riggs CD. 2006. Disruption of the *Arabidopsis* SMC4 gene, AtCAP-C, compromises gametogenesis and embryogenesis. *Planta* **223:** 990–997.

Simon L, Voisin M, Tatout C, Probst AV. 2015. Structure and function of centromeric and pericentromeric heterochromatin in *Arabidopsis thaliana*. *Front Plant Sci* **6:** 1049.

Smith SJ, Osman K, Franklin FC. 2014. The condensin complexes play distinct roles to ensure normal chromosome morphogenesis during meiotic division in *Arabidopsis*. *Plant J* **80:** 255–268.

Soppe WJ, Jasencakova Z, Houben A, Kakutani T, Meister A, Huang MS, Jacobsen SE, Schubert I, Fransz PF. 2002. DNA methylation controls histone H3 lysine 9 methylation and heterochromatin assembly in *Arabidopsis*. *EMBO J* **21:** 6549–6559.

Stroud H, Hale CJ, Feng S, Caro E, Jacob Y, Michaels SD, Jacobsen SE. 2012. DNA methyltransferases are required to induce heterochromatic re-replication in Arabidopsis. *PLoS Genet* **8:** e1002808.

Stroud H, Greenberg MV, Feng S, Bernatavichute YV, Jacobsen SE. 2013. Comprehensive analysis of silencing mutants reveals complex regulation of the *Arabidopsis* methylome. *Cell* **152:** 352–364.

Stroud H, Do T, Du J, Zhong X, Feng S, Johnson L, Patel DJ, Jacobsen SE. 2014. Non-CG methylation patterns shape the epigenetic landscape in *Arabidopsis*. *Nat Struct Mol Biol* **21:** 64–72.

Tanaka A, Tanizawa H, Sriswasdi S, Iwasaki O, Chatterjee AG, Speicher DW, Levin HL, Noguchi E, Noma K. 2012. Epigenetic regulation of condensin-mediated genome organization during the cell cycle and upon DNA damage through histone H3 lysine 56 acetylation. *Mol Cell* **48:** 532–546.

Uhlmann F. 2016. SMC complexes: from DNA to chromosomes. *Nat Rev Mol Cell Biol* **17:** 399–412.

Vazquez F, Vaucheret H, Rajagopalan R, Lepers C, Gasciolli V, Mallory AC, Hilbert JL, Bartel DP, Crete P. 2004. Endogenous *trans*-acting siRNAs regulate the accumulation of *Arabidopsis* mRNAs. *Mol Cell* **16:** 69–79.

Wang MH, Zhao YZ, Zhang B. 2015. Efficient test and visualization of multi-set intersections. *Sci Rep* **5:** 16923.

Wendte JM, Pikaard CS. 2017. The RNAs of RNA-directed DNA methylation. *Biochim Biophys Acta* **1860:** 140–148.

Williams BP, Pignatta D, Henikoff S, Gehring M. 2015. Methylation-sensitive expression of a DNA demethylase gene serves as an epigenetic rheostat. *PLoS Genet* **11:** e1005142.

Woo HR, Pontes O, Pikaard CS, Richards EJ. 2007. VIM1, a methylcytosine-binding protein required for centromeric heterochromatinization. *Genes Dev* **21:** 267–277.

Wood AJ, Severson AF, Meyer BJ. 2010. Condensin and cohesin complexity: the expanding repertoire of functions. *Nat Rev Genet* **11:** 391–404.

Woodcock CL, Ghosh RP. 2010. Chromatin higher-order structure and dynamics. *Cold Spring Harb Perspect Biol* **2:** a000596.

Zemach A, Kim MY, Hsieh PH, Coleman-Derr D, Eshed-Williams L, Thao K, Harmer SL, Zilberman D. 2013. The *Arabidopsis* nucleosome remodeler DDM1 allows DNA methyltransferases to access H1-containing heterochromatin. *Cell* **153:** 193–205.

Zhang X, Yazaki J, Sundaresan A, Cokus S, Chan SW, Chen H, Henderson IR, Shinn P, Pellegrini M, Jacobsen SE, et al. 2006. Genome-wide high-resolution mapping and functional analysis of DNA methylation in *Arabidopsis*. *Cell* **126:** 1189–1201.

Zhou M, Law JA. 2015. RNA Pol IV and V in gene silencing: rebel polymerases evolving away from Pol II's rules. *Curr Opin Plant Biol* **27:** 154–164.